This manuscript's first original version was submitted on March 8th 2023 for consideration in the peer-reviewed *Solar Energy* journal. Please note that the manuscript has not undergone peer-review yet and has not been formally accepted for publication. Subsequent versions of this manuscript may have slightly different content. Please feel free to contact the corresponding author; we welcome feedback.

Photosynthetically Active Radiation Separation Model for High-Latitude Regions

S. Ma Lu [1,*], D. Yang [2], M. C. Anderson [3], S. Zainali [1], B. Stridh [1], A. Avelin [1], P. E. Campana [1,*]

1 Mälardalen University, Department of Sustainable Energy Systems, Västerås, Sweden

2 School of Electrical Engineering and Automation, Harbin Institute of Technology, Harbin, Heilongjiang, China

3 USDA ARS, Hydrology and Remote Sensing Laboratory, Beltsville, MD, USA

Corresponding author: silvia.ma.lu@mdu.se

Abstract

Photosynthetically active radiation (PAR) is a key parameter for modelling the photosynthetic behaviour of plants in response to sunlight and, subsequently, for determining crop yield. Separating PAR into direct and diffuse components is of significance to agrivoltaic systems, which combine solar energy conversion and agricultural farming on the same portion of land. Placing photovoltaic on agricultural land results in varying shading conditions throughout the day and seasons, producing a higher contribution of incident diffuse PAR to the crops beneath the system in these shaded regions. Additionally, photosynthesis is more efficient under conditions of diffuse PAR than direct PAR per unit of total PAR. This work introduces a new separation model for PAR, which is able to accurately estimate diffuse PAR from the global one. The model modifies the YANG2 model, by adding four new predictors: the optical thickness of PAR, vapour pressure deficit, aerosol optical depth, and albedo of PAR. The proposed model has been calibrated, tested, and validated at three sites in Sweden with latitudes above 58° N, obtaining R^2 exceeding 0.91 and nRMSE less than 17%. Compared to YANG2, which was previously found to be a high-performance model, the new model is superior by up to 1% both in R^2 and nRMSE. Additionally, an analysis of the seasonal trends and variation of the different PAR components is provided to alleviate the dearth of PAR studies in high-latitude regions.

Keywords: photosynthetically active radiation, separation models, direct and diffuse, ICOS, CERES, agrivoltaics

1. Introduction

In land-based ecosystems, carbon uptake is primarily influenced by solar radiation during the daytime (Li et al., 2020). Photosynthetically active radiation (PAR) is the solar irradiance in the spectral interval between 400 and 700 nm (McCree, 1972, 1971). It plays an essential role in plant photosynthesis and associated processes, such as greenhouse gas generation by crops or biomass production (Keane et al., 2018; Tan et al., 2018). The knowledge of PAR helps one to estimate the plant's primary production (Mercado et al., 2009). Like the global horizontal irradiance (GHI), PAR can also be partitioned into its diffuse ($\mathrm{PAR_{diffuse}}$) and direct ($\mathrm{PAR_{direct}}$) components. This separation is of particular interest to many applications, especially for PAR estimation over land with complex topography, where the surrounding features can block the direct PAR component in an intricate and time-varying way (Olseth, 1997; Wang et al., 2006). Another application of this diffuse–direct separation of PAR is to study PAR distribution in plant canopies, where the diffuse light penetrates to a greater depth within the canopies than does the direct light (Mariscal et al., 2004). Furthermore, the light-use efficiency of plant canopies increases under cloudy conditions, due to the enhancement of the PAR diffuse component (Gu et al., 2002; Kanniah et al., 2012; Mercado et al., 2009). Li et al. (2020) studied the influence of diffuse PAR radiation in a desert steppe ecosystem and concluded that the maximum canopy photosynthesis was reached under cloudy skies.

The implication of PAR separation becomes more profound in the field of agrivoltaic systems. Agrivoltaic system is a novel concept, which combines solar photovoltaic and agricultural activities on the same land area. The agrivoltaic technology is an efficient, effective, and innovative solution to tackling land use competition (Adeh et al., 2019). Nonetheless, one important concern of using such systems is that, for the coexistence of solar energy and agricultural farming, crop yield must not go below tolerable limits. It is known that shading generally decreases crop yield, and different crops behave differently under shading conditions (Barron-Gafford et al., 2019). In open-field agrivoltaic systems, the amount of PAR reaching the agricultural land is not homogeneously distributed. The solar modules installed in the system produce variable levels of shading directly on the crops throughout a day and over a year. In these shaded areas, the diffuse component of PAR plays a dominant role. Therefore, knowing the amount of diffuse and direct PAR incident to a specific crop area beneath the agrivoltaic system implies a more accurate crop yield estimation. Noticeably, the study by Campana et al. (2021) was among the first works in agrivoltaic systems that introduced the concept of PAR separation for calculating crop yield; the topic of concern is an exceedingly recent one.

Despite the relevance of PAR on crop growth, the scarcity of PAR measurements and the lack of a worldwide measurement network with standardized quality control protocols (Ferrera-Cobos et al., 2020; Mizoguchi et al., 2010; Niu et al., 2019; Wang et al., 2016) directly explain the limited number of studies about PAR thus far as compared to, for example, to more extensive studies of GHI or diffuse horizontal irradiance (DHI). The lack of measurements is even more pronounced for the diffuse component of PAR. Therefore, as a work-around, several authors have suggested a variety of models to estimate the different components of PAR. PAR components can be estimated using atmospheric radiative transfer models

(ARTM), e.g., Bird and Riordan (1986), Gueymard (1995) or Emde et al. (2016) and methods derived from these, e.g., Wandji et al. (2019) or Thomas et al. (2019). However, since ARTM is associated with high complexity and using it demands much knowledge in atmospheric sciences, most of the models are empirical. These empirical models can derive the global component of PAR, and a limited number can also derive diffuse PAR (e.g., Weiss and Norman, 1985, Kathilankal et al., 2014), from parameters commonly measured at weather stations (e.g., Alados et al., 1996, Hu et al., 2007), from spectral band measurement (e.g., Trisolino et al., 2016), and from satellite data (e.g., Su et al., 2007, Janjai et al., 2011, Hao et al., 2019). The exhaustive review by Nwokolo et al. (2018) offers an overview of empirical models to estimate the global PAR (i.e., $\mathrm{PAR_{global}} = \mathrm{PAR_{diffuse}} + \mathrm{PAR_{direct}}$). It is worth mentioning that the correlation between PAR and meteorological parameters is location-dependent (García-Rodríguez et al., 2020).

Several works have focused on the ratio PAR/GHI and its behaviour in different climate zones. According to the review by Noriega et al. (2020), the ratio is typically higher during summer and lower during winter, though exceptions to this rule have been highlighted by Yu and Guo (2016) or and Ma Lu et al. (2022). Analysis of the PAR/GHI ratio under cloudless conditions shows a clear dependence on air mass (González and Calbó, 2002). However, under all-sky conditions, the dependence of the ratio is unclear. Yu et al. (2015), Akitsu et al. (2015), and, Ferrera-Cobos et al. (2020) observed a decrease in the ratio when the clearness index (i.e., $k_t = \mathrm{GHI/E_{ext}}$) increases. In contrary, Lozano et al. (2022) found no significant dependence of the ratio on k_t. Most research studies admit that the PAR/GHI ratio is location- and season-dependent (Hu et al., 2007; Jacovides et al., 2003; Li et al., 2010; Proutsos et al., 2022), therefore pointing out the need to further investigate the behaviour of the ratio at more sites with different climates around the globe.

The $\mathrm{PAR_{diffuse}}$ component is generally analysed by the PAR diffuse fraction (i.e., $k_{\mathrm{PAR}} = \mathrm{PAR_{diffuse}/PAR_{global}}$). Several models have been proposed to obtain k_{PAR} and most of them are inspired by GHI separation models, which estimate DHI from GHI, and their clearness index dependence (Gu et al., 1999; Jacovides et al., 2010; Kathilankal et al., 2014; Oliphant and Stoy, 2018; Ren et al., 2018). Since the spectral range of PAR is a portion of that of GHI, it is logically attractive to use just GHI separation models to partition $\mathrm{PAR_{global}}$. Indeed, the recent work by Ma Lu et al. (2022) applied and compared several GHI separation models for separating $\mathrm{PAR_{global}}$.

Generally, empirical models based on simple mathematical expressions reported in the literature are applicable when the local conditions are similar to those used for calibrating the models. However, a limited number of studies investigate the transferability of the models to other locations around the globe. For instance, de Blas et al. (2022) analysed the accuracy of 21 semi-empirical models of $\mathrm{PAR_{global}}$ in seven locations of the SURFRAD network in the United States that the authors claimed to be representative of a large variety of weather conditions. All 21 models use a combination of easily retrievable parameters (see section 3.1 for further details). The results show that calibrating the model parameters according to the studied locations can slightly improve the estimation of the PAR components. But since the global calibrated models already offer very satisfactory results, they should be chosen considering the availability of the input variables at each specific location. These findings, nevertheless, cannot necessarily be applied to high latitudes (>49°N), and to northern European countries where agrivoltaics research in these territories has expanded during the latest decade. There exists an overall lack of knowledge on the transferability and performance of PAR separation models in high-latitude environments.

In this work, a new separation model to estimate $\mathrm{PAR}_{\mathrm{diffuse}}$ is proposed. It is derived from the original YANG2 model (Yang and Boland, 2019), which is a GHI separation model, because of its high accuracy demonstrated for both GHI and $\mathrm{PAR}_{\mathrm{global}}$ (Ma Lu et al., 2022). In addition, the newly proposed model is based on atmospheric inputs conveniently retrievable from available databases, algorithms, and satellite-derived data. The study is done for three locations in Sweden, considering an evident gap in PAR separation model studies applied to northern latitudes exists. At the same time, an analysis of the seasonal trends and variation of the different PAR components is provided for these colder climates. Additionally, the authors are experimenting with agrivoltaic systems facilities based in Sweden. Hence, it is a priori opportune to explore and be able to apply the developed model in situ in the upcoming future.

The remainder of the study is organized as follows: Section 2 presents the meteorological data used for developing, calibrating, testing, and validating the model proposed in this study. Section 3 describes the steps taken to develop the new separation model. Section 4 evaluates the performance of the proposed model and discusses the results obtained for the selected sites. More specifically, an analysis of the fluctuations in PAR components in these high-latitude locations is presented and discussed. Section 5 concludes the study.

2. Weather Data

The dataset used in this work for training and testing the proposed PAR separation model consists of multiple-year measurements of $\mathrm{PAR}_{\mathrm{global}}$ and $\mathrm{PAR}_{\mathrm{diffuse}}$ among other variables from the Integrated Carbon Observation System in Sweden (ICOS Sweden, 2022) network. Three locations in Sweden with available measurements were selected, namely, Lanna, Degerö, and Norunda (Figure 1). The dataset spans three years of data for each station with a time resolution of 30 min. Since the measurements of PAR from ICOS stations are in units of flux density as a quantum process (PPFD), a conversion factor of $1\ \mathrm{W/m^2} \approx 4.6\ \mathrm{\mu mol/m^2/s}$ (Langhans et al., 1997) is applied whenever required. The data for each location is divided into two subsets. On one hand, the training set consists of two years of data, which is used to fit the separation model parameters for the site. On the other hand, the validation (or testing) set consists of the remaining one year of data, which is used to test the fitted models with unseen data for the location of concern. The metadata of the sites considered in this study is tabulated in Table 1. A complete list of the available variables from these locations of the ICOS Sweden network is provided in section 3.2.

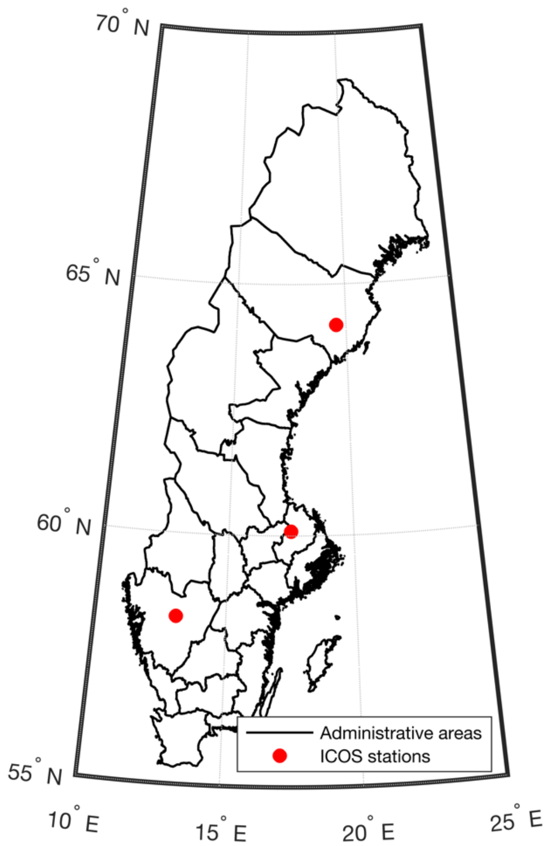

Figure 1. Map of Sweden with the location of the ICOS Sweden network stations selected for the analysis. Map source: *(GADM, 2022)*.

Table 1. Information about the study locations and details of the data extracted from ICOS-Sweden network. The last column indicates the numbers of train/test samples (or data points) at each location after quality control (described in section 2.2).

Station	**Latitude (ºN)**	**Longitude (ºE)**	**Elevation (m)**	**Data period**	**Samples training/ testing**
Lanna	58º20'	13º06'	75	2016-2018	7062/ 3618
Degerö	64º18'	19º55'	270	2016- 2018	6993/ 2117
Norunda	60º05'	17º29'	46	2016-2018	5727/ 2676

2.1. Auxiliary Data

Besides $\mathrm{PAR_{global}}$ and $\mathrm{PAR_{diffuse}}$, separation models often require as input several auxiliary variables, which are often computable or can be accessed for general time periods and locations. These auxiliary variables are described in this section. Firstly, the extraterrestrial radiation (E_{ext}) on a horizontal plane, which is needed to compute k_t, is calculated as explained in Duffie & Beckman (2013). It is noted that the computation of E_{ext} requires further a parameter known as the solar constant (*SC*), which is here in taken to be $SC = 1361.1\ \mathrm{W/m^2}$, following Gueymard (2018). Moreover, the Earth's orbit eccentricity correction factor is used as per the definition by Spencer's equation (Spencer, J. W, 1971). Extraterrestrial PAR ($\mathrm{PAR_{ext}}$) is calculated analogously to E_{ext}, but with the approximated PAR solar constant, which is $\mathrm{PAR_{SC}} = 634.4\ \mathrm{W/m^2}$ (Iqbal, 1983).

The solar zenith angle is calculated from the solar elevation and the latter is derived using the solar positioning algorithm developed by Koblick (2021). Moreover, to account for the atmospheric refraction effects, the model from the ESRL Global Monitoring Laboratory (US Department of Commerce, 2021) is applied to correct the solar elevation angle. Both the clear-sky GHI ($\mathrm{G_{cs}}$) and clear-sky PAR ($\mathrm{PAR_{cs}}$) are acquired from the Clouds and the Earth's Radiant Energy System (CERES) satellite-based observations (Wielicki et al., 1996). Both satellite-derived diffuse fraction of GHI and the diffuse fraction of PAR are obtained from the CERES SYN1deg Ed. 4.1 product (Doelling, 2017). CERES offers hourly satellite-derived GHI, DHI, PAR total, and PAR diffuse from March 2000 till March 2022 with global coverage with a 1° x 1° resolution in both latitudes and longitudes. All satellite-derived data is downloaded to match the spatial locations and temporal range of the measured ICOS data.

It should be noted that even though ICOS data has a temporal resolution of 30 min, due to the shortest time step availability of CERES data, which has an hourly resolution at the midpoint, the remaining part of this work (including both analysis and results) is performed with a 1-hour time step. In the present study, the half-hourly time stamps of the 30-min data points from ICOS are taken (i.e., 9:30, 10:30, 11:30, and so forth).

2.2. Quality control

Quality control (QC) constitutes an essential part of radiation modelling, with the goal of filtering and eliminating spurious and erroneous data points. Since the observational data are to be used for the determination of fitting parameters, validation, and performance comparison of the separation models, QC must be applied to ensure that exclusively the highest-quality data points are selected. That said, there is no ideal or universally accepted QC procedure for broadband irradiance data, not to mention PAR data. This issue has been pointed out in the introduction section and in the previous work by Ma Lu et al. (2022). On that account, the previously used QC procedure for PAR is adopted for this work as well. The reader is referred to the previous publication for a detailed list of quality filters (Ma Lu et al., 2022). The only added quality filter corresponds to albedo for which data with values greater than one was rejected.

3. Methodology

Before the development of the new PAR separation model is revealed, it is important to conduct a literature review on studies that highlighted influencing atmospheric parameters to PAR components, and particularly to $\mathrm{PAR}_{\mathrm{diffuse}}$. Subsequently, a correlation analysis is conducted between the diffuse fraction of PAR and various meteorological variables available from the ICOS Sweden network to identify highly correlated parameters. This correlation analysis was extended to include variables drawn from the first-step screening and not provided by the ICOS Sweden network. Based on the correlation analysis, a selection of new predictors results. The new separation model, which is based on the YANG2 model (Yang and Boland, 2019), is then developed in the third step, with consideration to those chosen predictors resulting from the second step. Finally, the last two steps are to fit the model coefficients using the experimental data and to evaluate the performance of the new model. A further comparison is made to two existing models, i.e., YANG2 and STARKE, which were previously found to be the most accurate. A graphical summary of the methodology is presented in Figure 2.

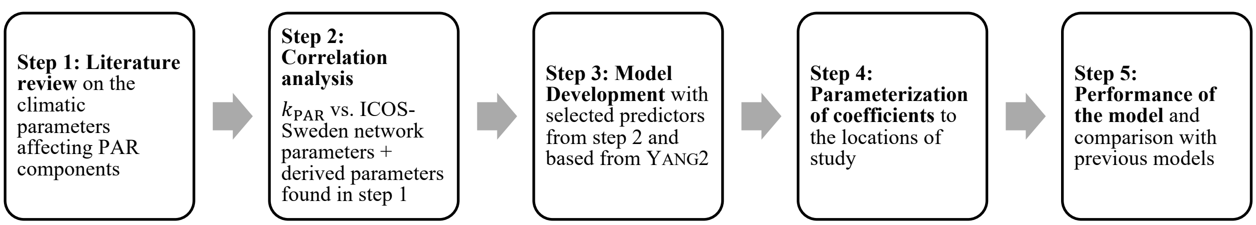

Figure 2. Schematic diagram of the workflow applied in this work for the development of a new PAR separation model.

3.1 Literature review on the climatic parameters affecting PAR diffuse

An initial literature review has been performed to analyse which atmospheric variables are most influencing the ecosystem production efficiency and, thus, the PAR components.

In the study by Li et al. (2020), in a desert steppe ecosystem, lower vapour pressure deficit (VPD ≤ 1 kPa), lower air temperature (Ta < 20°C) and non-stressed water conditions were more favourable conditions for enhanced ecosystem photosynthesis under cloudy skies ($k_t < 0.7$). $\mathrm{PAR}_{\mathrm{diffuse}}$ peaked when k_t was around 0.5.

A work by Lu et al. (2022) using data from 40 sites around the globe has concluded that VPD and soil moisture (SM) are significant variables in ecosystem production efficiency that should be fairly valued in ecosystem modelling. For most of the studied sites, high VPD values cause positive changes in PAR while low SM values cause negative changes in the fraction of PAR absorbed by the plants (fPAR). The study underlines the influence of VPD on incident PAR in a multitude of locations. Yet none of those sites was in northern latitudes.

A new method to estimate PAR values for clear-sky conditions used solar zenith angle, total column contents of ozone (TOC) and water vapour (TWV), aerosol optical depth (AOD), vertical profiles of temperature, pressure, density and volume mixing ratio of gases, elevation and ground albedo as inputs (Wandji Nyamsi et al., 2019). The study emphasized that the errors in the suggested method were caused by the overestimation of the input variables AOD and the assumption of constant $\mathrm{PAR}_{\mathrm{albedo}}$, suggesting these two variables have a significant effect on the PAR under clear skies.

Recent work by de Blas et al. (2022), analysed $\mathrm{PAR}_{\mathrm{global}}$ estimations at 1-min, hourly, and daily time steps at seven sites from 21 models that use a combination of the following meteorological parameters: GHI, clearness index, diffuse fraction, vapour pressure, relative optical air mass, precipitable water, solar zenith angle, sky's brightness, and sky's clearness. The work further analysed the performance of the models for different groups of sky conditions (clear to overcast) and found that for some models, the accuracy worsened when applied to overcast skies.

Another recent work by Proutsos et al. (2022) studied the atmospheric factors affecting the PAR/GHI ratio in a Mediterranean site. The authors concluded that the atmospheric water content (expressed by the degree of cloudiness, actual water vapour, optical thickness, or dew point temperature) and the clearness index were the most influential factors in the ratio. Air temperature and related meteorological variables (relative humidity, vapour pressure deficit and saturation vapour pressure) were found to have no significant effect on the ratio.

Regarding PAR diffuse estimations, the latest work by Lozano et al. (2022) found a clear dependence of the k_{PAR} on the clearness index and total cloud cover (TCC) at a Mediterranean site. The authors proposed a model to estimate k_{PAR} obtained through the first adaptation of the Boland-Ridley-Lauret (BRL) model (Ridley et al., 2010) based on the clearness index, solar elevation angle, apparent solar time (AST), daily clearness index and persistence index. When fitting the model to the studied site, the authors found that AST and daily clearness index were insignificant and suggested these terms be removed from the model.

Kathilankal et al. (2014) developed a semi-parametric PAR separation model for the United States. It adapts the BRL model using physically viable climate variables as predictors: relative humidity, PAR clearness index, surface albedo and solar elevation angle. The proposed model takes a conditional approach, which uses two logistic fits, one for clear-sky conditions and the other for cloudy conditions.

3.2 Correlation Analysis

The second step is to perform a correlation analysis between the observed diffuse fraction of PAR to each of the meteorological variables available from the selected ICOS Sweden network stations (see Table 2), and the derived potential variables that could benefit the separation model (see Table 3). The derived variables are selected according to the literature review presented above. The correlation analysis of the meteorological variables to k_{PAR} was used to rule out variables that are not important predictors of k_{PAR}, double-check variables considered already in well-known models, and to detect potential new significant variables, either based on Pearson's correlation coefficient or visually from the scatterplot pattern (Appendix A1). The analysis is performed with hourly data. Shape-preserving piecewise cubic interpolation is used when the availability of the data has a larger timestep than hourly (e.g., AOD).

Table 2. List of variables available from the ICOS Sweden network Lanna, Degerö and Norunda stations for the period of 2016-2018 (“ICOS Sweden,” 2022).

Variable name	Variable description	Unit	Quantity kind
Swin_p	incoming shortwave radiation, pyranometer	W m-2	energy flux
Lwin	incoming long-wave radiation, net radiometer	W m-2	energy flux
Lwnet	net long-wave radiation, net radiometer	W m-2	energy flux
Lwout	outgoing long-wave radiation, net radiometer	W m-2	energy flux
NetRad	net radiation, net radiometer	W m-2	energy flux
PPFD_DIFF	photosynthetic photon flux density diffuse	µmol m-2 s-1	particle flux
PPFD_DIR	photosynthetic photon flux density direct	µmol m-2 s-1	particle flux
PPFD_IN	photosynthetic photon flux density incoming	µmol m-2 s-1	particle flux
PPFD_OUT	photosynthetic photon flux density outgoing	µmol m-2 s-1	particle flux
P	precipitation (total)	mm	length
Pa	air pressure	hPa	pressure
RH	relative humidity	%	portion
Sun	sunshine duration, sunshine sensor	1	portion
Swin_n	incoming shortwave radiation, net radiometer	W m-2	energy flux
Swnet_n	net shortwave radiation, net radiometer	W m-2	energy flux
Swout_n	outgoing shortwave radiation, net radiometer	W m-2	energy flux
T_canopy	target surface temperature	°C	temperature
Ta	air temperature	°C	temperature
H[1]	sensible heat flux	W m-2	energy flux
LE[1]	latent heat flux	W m-2	energy flux
Fc[1]	carbon dioxide (CO2) flux	µmol m-2 s-1	particle flux
Fn2o[1,2]	nitrous oxide (N2O) flux	µmol m-2 s-1	particle flux
Ustar[1]	friction velocity	m s-1	velocity
WS[1]	wind speed	m s-1	velocity
WD[1]	wind direction	°	angle
NEE[1]	net ecosystem exchange	µmol m-2 s-1	particle flux
LE_f[1]	gap-filled latent heat flux	W m-2	energy flux
H_f[1]	gap-filled sensible heat flux	W m-2	energy flux

[1] Variables not available in Degerö ICOS station.
[2] Variable only available in Lanna ICOS station.

Table 3. List of variables investigated through correlation analysis for the development of the new separation model of PAR based on the findings provided in the literature review.

Variable name	Variable description	Unit	Derived from	Source
Alb	surface albedo	-	$\mathrm{Alb} = \frac{\mathrm{Swout\_n}}{\mathrm{Swin\_n}}$	
$\mathbf{PAR_{albedo}}$	surface PAR albedo	-	$\mathrm{PAR_{albedo}} = \frac{\mathrm{PPFD\_OUT}}{\mathrm{PPFD\_IN}}$	
AM	air mass	-	$\mathrm{AM} = \frac{1}{\cos(Z) + 0.50572 * (6.07995 + (90 - Z))^{-1.6364}}$	(Kasten and Young, 1989)
$\boldsymbol{e_a}$	actual vapor pressure	mbar	$e_a = e_s * \frac{\mathrm{RH}}{100}$	(Technical Committee on Standardization of Reference Evapotranspiration, 2005)

$\boldsymbol{e_s}$	saturation vapor pressure	mbar	$e_s = 6.1078 * \exp\left(\frac{17.27 * \mathrm{Ta}}{\mathrm{Ta} + 237.3}\right)$	(Technical Committee on Standardization of Reference Evapotranspiration, 2005)
VPD	vapor pressure deficit	mbar	$\mathrm{VPD} = e_s - e_a$	
$\boldsymbol{\delta}$	optical thickness	-	$\delta = \ln\left(\frac{E_{\mathrm{ext}}}{\mathrm{GHI}}\right)$	(Proutsos et al., 2022)
$\boldsymbol{\delta_{\mathrm{PAR}}}$	PAR optical thickness	-	$\delta_{\mathrm{PAR}} = \ln\left(\frac{\mathrm{PAR_{ext}}}{\mathrm{PAR_{global}}}\right)$	
$\mathbf{T_{dew}}$	dew point temperature	°C	$X = \frac{17.27 * \mathrm{Ta}}{\mathrm{Ta} + 237.3} + \ln\left(\frac{\mathrm{RH}}{100}\right)$ $\mathrm{T_{dew}} = \frac{237.3 * X}{17.27 - X}$	(Barenbrug, 1974)
AOD	total aerosol optical depth 550 nm	-	CAMS-AOD satellite-derived service provided by ECMWF. Time coverage from 2004-01-01 up to current day-2. Time step of 3 h.	(ECMWF, 2022)

From the analysis, the variables sunshine duration (Sun) and the PAR optical thickness (δ_{PAR}) were identified as having a high degree of correlation to k_{PAR}. Despite sunshine duration exhibits the highest correlation to k_{PAR}, the variable is not considered as a new predictor due to the difficulty in obtaining it. In addition, even though exhibiting moderate to lower degrees of linear correlation (Table 4), the following variables VPD, AOD, and $\mathrm{PAR_{albedo}}$ are selected. These variables have been shown to influence either $\mathrm{PAR_{diffuse}}$ or k_{PAR} based on the previous literature review (Li et al., 2020; Lu et al., 2022; Wandji Nyamsi et al., 2019). The correlation coefficients of the selected variables are also shown for the datasets of Degerö and Norunda sites (Table 4).

Table 4. Pearson's correlation coefficients of the variables added to the new separation model of PAR for the data of the three studied locations described in Table 1.

	Pearson's correlation coefficient to $\boldsymbol{k_{\mathrm{PAR}}}$		
Variable	**Lanna**	**Degerö**	**Norunda**
$\boldsymbol{\delta_{PAR}}$	0.8111	0.7907	0.8453
VPD	-0.5478	-0.5329	-0.4373
AOD	0.2613	0.2353	0.2873
$\mathbf{PAR_{albedo}}$	0.1360	0.1200	0.0902

3.3 Model development

YANG2 (Yang and Boland, 2019), which is a logistic form model, has been selected as the starting point for developing the new PAR separation model. The logistic form is chosen based on the agreement in the literature as yielding higher accuracy for both for separation models of GHI and separation models of PAR in comparison with other functional shapes. Previous work by Ma Lu et al. (2022) showed that YANG2 and STARKE (Starke et al., 2018) were among the best-performing models to obtain $\mathrm{PAR_{diffuse}}$ from $\mathrm{PAR_{global}}$. It should be noted that both YANG2 (Eq.1) and STARKE (Eq.4) were originally developed for decomposing GHI. For this reason, Ma Lu et al. (2022) have applied the Spitters relationship (Eq.6) (Spitters et al., 1986) to expand the applicability of these models to PAR separation.

$$k^{\text{YANG2}} = C + \frac{1-C}{1+e^{\beta_0+\beta_1 k_t+\beta_2 \mathrm{AST}+\beta_3 Z+\beta_4 \Delta k_{tc}+\beta_6 k^{(s)}}} + \beta_5 k_{de}, \tag{1}$$

$$\Delta k_{tc} = k_{tc} - k_t = \frac{G_{\mathrm{cs}}}{E_{\mathrm{ext}}} - k_t, \tag{2}$$

$$k_{de} = \max\left(0, 1 - \frac{G_{\mathrm{cs}}}{\mathrm{GHI}}\right), \tag{3}$$

$$k^{\text{STARKE}} = \begin{cases} \dfrac{1}{1+e^{\beta_7+\beta_8 k_t+\beta_9 \mathrm{AST}+\beta_{10} Z+\beta_{11} K_T+\beta_{12}\psi+\frac{\beta_{13} G_{\mathrm{cs}}}{277.78}}}, k_{\mathrm{CSI}} \geq 1.05 \text{ and } k_t > 0.65; \\ \dfrac{1}{1+e^{\beta_0+\beta_1 k_t+\beta_2 \mathrm{AST}+\beta_3 Z+\beta_4 K_T+\beta_5\psi+\frac{\beta_6 G_{\mathrm{cs}}}{277.78}}}, \text{otherwise} \end{cases} \tag{4}$$

$$K_T = \frac{\sum_{n=1}^{24} \mathrm{GHI}_n}{\sum_{n=1}^{24} E_{\mathrm{ext}_n}}, \tag{5}$$

$$k_{\mathrm{PAR}}^{\mathrm{model}} = \frac{\mathrm{PAR_{diffuse}}}{\mathrm{PAR_{global}}} = \frac{\left[1+0.3\left(1-(k^{\mathrm{model}})^2\right)\right]k^{\mathrm{model}}}{1+(1-(k^{\mathrm{model}})^2)\cos^2(90-\beta)\cos^3\beta} \tag{6}$$

Briefly, k_t is the clearness index, G_{cs} is the clear-sky GHI [W/m^2], Z is the solar zenith angle [°], AST is the apparent solar time [h], E_{ext} is the extraterrestrial radiation [W/m^2], $k^{(s)}$ is the satellite-derived diffuse fraction, K_T is the daily clearness index, the ψ predictor is the three-point moving average of clearness index, k_{CSI} is the clear-sky index, and β is the solar elevation angle [º].

In the present work, the model form of YANG2 is taken as a basis but with all the predictors adapted into PAR (i.e., k_t to k_{t_PAR}, Δk_{tc} to $\Delta k_{tc\_\mathrm{PAR}}$). The following model, hereafter called CLY (i.e., an abbreviation of the main developers' family names in alphabetical order), is proposed by including the four new relevant variables found in the previous subsection (see Table 4).

$$k_{\mathrm{PAR}}^{\mathrm{CLY}} = C + \frac{1-C}{1+e^{\beta_0+\beta_1 k_{t\_\mathrm{PAR}}+\beta_2 \mathrm{AST}+\beta_3 Z+\beta_4 \Delta k_{tc_{PAR}}+\beta_5 \mathrm{PAR_{albedo}}+\beta_6 \delta_{\mathrm{PAR}}+\beta_7 \mathrm{AOD}+\beta_8 \mathrm{VPD}+\beta_{10} k_{\mathrm{PAR}}^{(s)}}} + \beta_9 k_{de\_\mathrm{PAR}}, \tag{7}$$

where,

$$k_{t\_\mathrm{PAR}} = \frac{\mathrm{PAR_{total}}}{\mathrm{PAR_{ext}}} \tag{8}$$

$$k_{de\_\mathrm{PAR}} = \max\left(0, 1 - \frac{\mathrm{PAR_{cs}}}{\mathrm{PAR}}\right) \tag{9}$$

$$\Delta k_{tc\_\mathrm{PAR}} = \frac{\mathrm{PAR_{cs}}}{\mathrm{PAR_{ext}}} - k_{t\_\mathrm{PAR}}, \tag{10}$$

Similarly, k_{t_PAR} is the PAR clearness index, $\mathrm{PAR_{cs}}$ is clear sky PAR [W/m^2], $\mathrm{PAR_{ext}}$ is the extra-terrestrial PAR [W/m^2] and $k_{\mathrm{PAR}}^{(s)}$ is the satellite-based diffuse fraction of PAR. The use of satellite-derived predictors was introduced by Yang and Boland (2019). Satellite-based predictors are efficient in illustrating the low-frequency variability of the diffuse component since they are based on physical models.

The proposed model (CLY) is evaluated for the selected locations in Section 2 and the performance compared to the original YANG2 and STARKE along with all PAR version of YANG2 and STARKE, which are annotated with an asterisk, i.e., YANG2* (Eq.11) and STARKE* (Eq.12):

$$k_{\mathrm{PAR}}^{\mathrm{YANG2}*} = C + \frac{1 - C}{1 + e^{\beta_0 + \beta_1 k_{t\_\mathrm{PAR}} + \beta_2 \mathrm{AST} + \beta_3 Z + \beta_4 \Delta k_{tc\_\mathrm{PAR}} + \beta_6 k_{\mathrm{PAR}}^{(s)}}} + \beta_5 k_{de\_\mathrm{PAR}}, \tag{11}$$

$$k_{\mathrm{PAR}}^{\mathrm{STARKE}*} = \begin{cases} \dfrac{1}{1 + e^{\beta_7 + \beta_8 k_{t\_\mathrm{PAR}} + \beta_9 \mathrm{AST} + \beta_{10} Z + \beta_{11} K_{T\_\mathrm{PAR}} + \beta_{12} \psi_{\mathrm{PAR}} + \frac{\beta_{13} \mathrm{PAR_{cs}}}{277.78}}}, k_{\mathrm{CSI\_PAR}} \geq 1.05 \text{ and } k_{t\_\mathrm{PAR}} > 0.65; \\ \dfrac{1}{1 + e^{\beta_0 + \beta_1 k_{t\_\mathrm{PAR}} + \beta_2 \mathrm{AST} + \beta_3 Z + \beta_4 K_{T\_\mathrm{PAR}} + \beta_5 \psi_{\mathrm{PAR}} + \frac{\beta_6 \mathrm{PAR_{cs}}}{277.78}}}, \text{otherwise} \end{cases} \tag{12}$$

3.4 Statistical indicators for the assessment of the models

The performance of the proposed CLY model (Eq.7) is evaluated at the different sites introduced in Section 2 using several popular error metrics. The results are then compared to the performances of the original and reparametrized YANG2 and STARKE models applied to PAR, as described in the work by Ma Lu et al. (2022). In addition, the proposed CLY model is compared to the reparametrized YANG2* and STARKE* models with all predictors adapted to PAR, as noted in section 3.3.

The error metrics selected in this work are the ones utilized by Ma Lu et al. (2022): the normalized mean bias error (nMBE), the normalized root mean square error (nRMSE), and the coefficient of determination (R^2). The observations of k_{PAR} are derived from the measurements of $\mathrm{PAR_{global}}$ and $\mathrm{PAR_{diffuse}}$ at the studied ICOS stations. The predictions are the $k_{\mathrm{PAR}}^{\mathrm{model}}$ calculated from the models.

3.5 Reparameterization of coefficients

The training datasets listed in Table *1* for the three locations under study are utilized to estimate locally fitted coefficients for each of the analysed models. To achieve this, a nonlinear optimization solver-based approach is employed, as detailed in Ma Lu et al. (2022). In this study, the root mean square error (RMSE) of k_{PAR} is selected as the target function to be minimized. This choice aligns with the statistical concept of consistency (Gneiting, 2011), as one of the main evaluation metrics is the nRMSE (section 3.4). The concept of consistency has been emphasized in previous research for the calibration and evaluation of point forecasts (Yang et al., 2020; Yang and Kleissl, 2022).

4. Results and discussion

4.1 CLY separation model performance

The proposed CLY satellite-augmented model for estimating diffuse PAR is evaluated alongside four other models at the three studied locations, using hourly data. These include the original YANG2 and STARKE GHI decomposition models with Spitters amendment for PAR, as well as the modified versions of YANG2* (Eq.11) and STARKE* (Eq.12) presented in Section 3.3. Table *5* presents the models' performances.

Table 5. The nRMSE [%], nMBE [%] and R^2 in predicted hourly diffuse PAR from of the proposed PAR separation model, CLY, compared to the other 2 models with different versions, Yang2* and Starke* with PAR predictors, and the original Yang2 and Starke applied to PAR as presented in Ma Lu et al. (2022). Locally fitted coefficients (using training data over 2-years, period 2016-2017) and validated (using testing data over 1-year, period 2018) at 3 ICOS-Sweden stations (Lanna, Degerö, Norunda). The errors are computed between the predicted and measured hourly PAR diffuse fraction values. Boldface denotes the best-performing model in a row.

Station	**CLY**	**STARKE***	**YANG2***	**STARKE**	**YANG2**
			nRMSE [%]		
Lanna	**12.86**	15.29	13.92	15.00	13.71
Degerö	16.64	18.43	**16.24**	20.00	17.99
Norunda	**14.89**	16.03	15.12	17.18	15.96
			nMBE [%]		
Lanna	**0.8**	-1.14	0.42	-1.87	-1.06
Degerö	-0.37	-1.89	0.14	-1.86	**-0.01**
Norunda	-1.85	**-0.89**	-1.13	-1.80	-1.74
			R^2		
Lanna	**0.94**	0.91	0.93	0.92	0.93
Degerö	**0.91**	0.89	**0.91**	0.87	0.90
Norunda	**0.92**	0.91	**0.92**	0.90	0.91

For two of the investigated locations with latitudes higher than 58° N, the CLY model's accuracy in terms of nRMSE and R^2 is superior to the other models. However, for Degerö, CLY performs slightly worse than YANG2 in terms of nRMSE. The added predictors to the YANG2 model, namely optical thickness, vapour pressure deficit, aerosol optical depth, and PAR albedo, can better represent the scattered processes in the atmosphere compared to the other models (Figure 3). Particularly, the CLY model outperforms other models (YANG2* and YANG2) in predicting clear-sky conditions when k_t values are between 0.7 and 0.8, and k_{PAR} values are lower than 0.2. An exception is observed in Degerö, where the behaviour is rather similar to YANG2. When compared to STARKE* and STARKE models, the CLY model estimates the shape of the envelope and the larger spread of data during partly cloudy conditions ($0.3 < k_t < 0.7$) in a superior way. The CLY model coefficients are presented in Table 6.

Table 6. Model coefficients of the proposed CLY PAR separation model fitted to the 3 ICOS stations in Sweden with hourly time step (Lanna, Degerö, and Norunda) each with 2 years of data for the period 2016-2017.

Station	C	β_0	β_1	β_2	β_3	β_4	β_5	β_6	β_7	β_8	β_9	β_{10}
Lanna	0.1084	4.6754	-0.0111	-0.0683	0.0001	-2.8288	-1.4563	-2.5791	-1.2877	0.0245	0.2520	-2.1574
Norunda	0.0933	4.3594	-0.9755	-0.0590	0.0105	-2.0031	-0.4034	-3.2240	-1.0686	0.0427	0.2883	-1.8674
Degerö	0.1514	3.2011	1.5564	-0.0486	0.0079	-2.1034	-0.3636	-2.5949	-0.5795	0.0475	0.4814	-2.1945

Results show that predicting k_{PAR} is more accurate when using PAR-derived predictors (Yang2*) than GHI-derived predictors added to the Spitters relationship for Yang2. However, this trend is not observed for Starke*, which does not seem to outperform Starke. The reason could be due to the $k_{\mathrm{CSI\_PAR}}$ and k_{t_PAR} constraint values not being recomputed for the PAR-derived predictors.

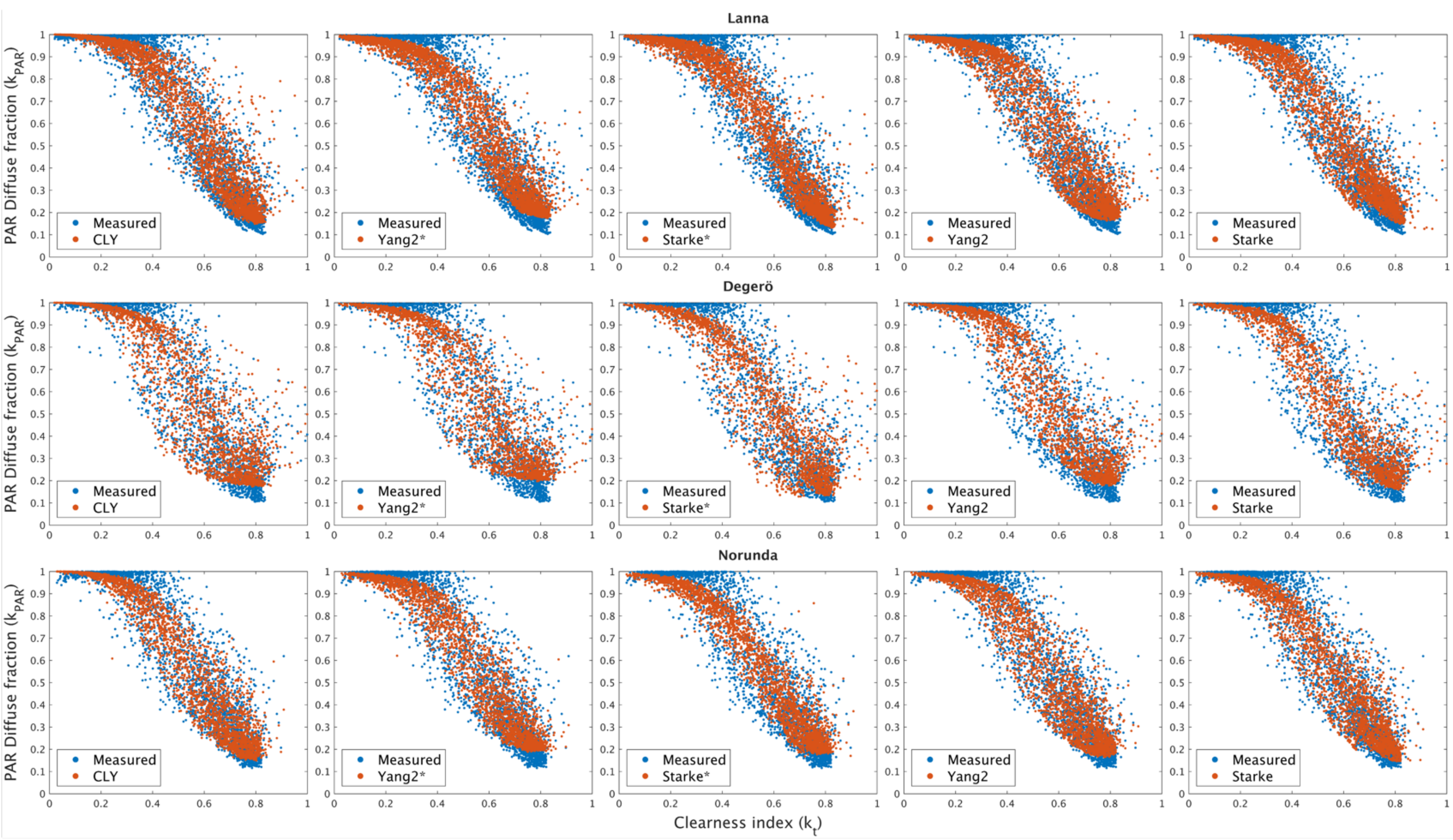

Figure 3. PAR diffuse fraction measured data plotted against the clearness index for the studied locations: Lanna (top row), Degerö (middle row), and Norunda (bottom row). The estimated results from the proposed PAR separation model CLY, Yang2* and Starke* with PAR predictors, and the original Yang2 and Starke applied to PAR are overlaid. The total number of data points in each plot refers to the testing data sample listed in Table 1.

Despite having several predictors, the proposed model is potentially widely applicable thanks to the availability of satellite data. Complete data needed for the model can be easily retrieved from satellite-derived data products or calculated using mathematical relationships from commonly available weather data (Section 3).

This work introduces a new PAR separation model developed and applied for northern latitudes to support the development of the agrivoltaic sector. In particular, to accurately determine the $PAR_{diffuse}$ reaching the crops beneath an agrivoltaic system from PAR_{global} measurements. The proposed model could be applied to other latitudes and climates to evaluate its worldwide performance, although this is beyond the scope of the present study.

4.2 PAR_{global}, PAR_{direct}, and $PAR_{diffuse}$ variation at northern latitudes

As highlighted in the introduction, studies on the behavior of PAR components for high-latitude regions are lacking. The annual evolution for PAR_{global}, PAR_{direct} and $PAR_{diffuse}$ measured at the ICOS sites at the three study locations is depicted in Figure 4. The monthly distribution of PAR_{global} shows a clear cycle, with maximum mean and median values around May and July for all locations, and the lowest values during winter. This seasonality trend is similarly observed in other studies for the northern hemisphere, such as the study by Lozano et al. (2022) in Granada, Spain (37.16° N, 3.61° W). However, the magnitude of PAR_{global} differs. In the Mediterranean location, the PAR_{global} during the warmest months exhibited values higher than 250 W/m^2, while the maximum in the Scandinavian sites was around 150 W/m^2 (with the exception of 2018, which reached average values slightly below 200 W/m^2). Moreover, the Lanna station, located at the southernmost latitude, received on average 30.64% more annual PAR_{global} radiation than Degerö, located 6° further north, for the period 2016-2017.

The seasonal pattern of the PAR_{direct} component exhibits the highest variation and distribution. The direct component is clearly influenced by the Sun's position and the intensity of the incoming light. It is worth noting that 2016 and 2017 present similar distributions, while 2018 shows a significantly different distribution. The atypical behaviour is aligned with the drought that occured in Sweden in 2018. The country experienced an earlier onset of summer at the start of May, which lasted throughout the summer months, with short interruptions mainly in June (Wilcke et al., 2020). For the three locations investigated, the average PAR_{direct} value was 57.48% higher in May 2018 than in the previous two years. The increased solar irradiance in 2018 was caused by the anomalous presence of clear sky conditions (Räisänen, 2019; Sinclair et al., 2019).

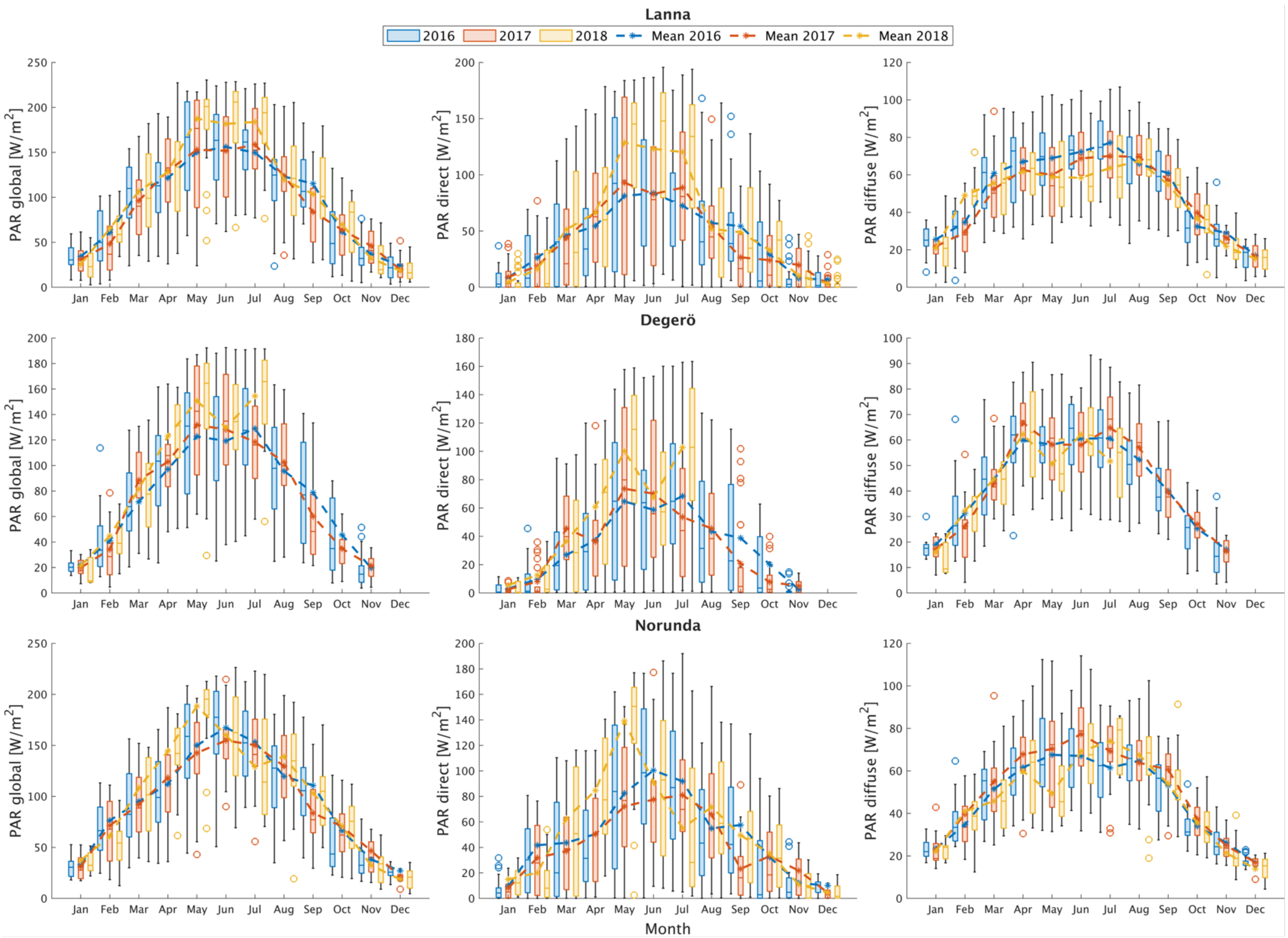

Figure 4. Monthly variation statistics for PAR_{global}, PAR_{direct} and $PAR_{diffuse}$ during the period 2016 – 2018 at the studied ICOS Sweden network stations: Lanna (top), Degerö (middle), and Norunda (bottom). For each box, central lines are the median, and upper and lower limits represent the percentiles 75th and 25th respectively. The limits of the segments represent the minimum and the maximum daily average values. The stars are the mean monthly values.

The monthly variation observed in Figure 4 for $PAR_{diffuse}$ is less pronounced than for PAR_{direct} or PAR_{global}. The main reason is the high complexity of the scattering processes involved in the diffuse component, affected by the presence of clouds, aerosols, surface albedo, and altitude. For the investigated sites, the trend is similar for all the years with a slight alteration in 2018 due to decreased amount of clouds, which brought overall lower values of $PAR_{diffuse}$. The annual mean $PAR_{diffuse}$ value for the locations studied was 46.65 W/m^2, marginally lower (59 W/m^2) than the one reported by Lozano et al. (2022) in Granada (Spain) 2008-2018 and higher (35 W/m^2) than the one reported by Trisolino et al. (2018) in Lampedusa (Italy) 2002-2016. Since there are scarce studies about PAR trends, the comparison is made to available studies in these Southern European locations. It is interesting to observe that the $PAR_{diffuse}$ is rather similar regardless of whether it is in the north or south of Europe.

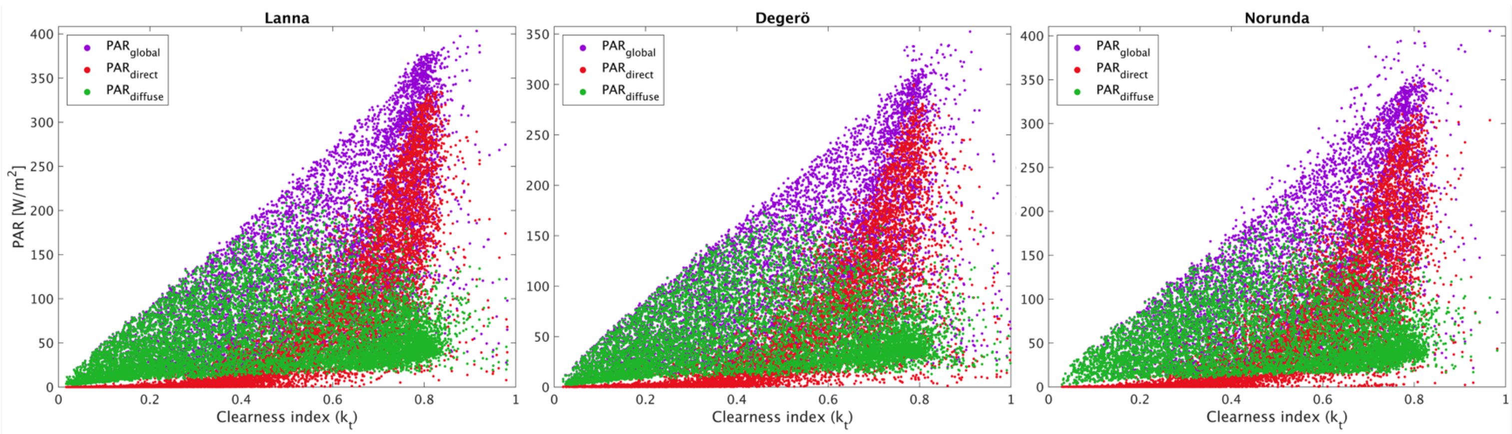

Figure 5. Scatterplots between the clearness index and $\mathrm{PAR_{global}}$, $\mathrm{PAR_{direct}}$ and $\mathrm{PAR_{diffuse}}$ for the period 2016 – 2018 at the studied ICOS Sweden network stations: Lanna (left), Degerö (middle), and Norunda (right). Hourly values at midpoint are used.

Figure 5 presents the effect of cloudiness on $\mathrm{PAR_{global}}$, $\mathrm{PAR_{direct}}$ and $\mathrm{PAR_{diffuse}}$ measurements for the investigated sites during the studied period. The upper envelope of $\mathrm{PAR_{global}}$ increases linearly with the clearness index. When the clearness index is low, $k_t < 0.3$, corresponding to thick cloud conditions (Chen et al., 2009), $\mathrm{PAR_{diffuse}}$ makes the primary contribution to $\mathrm{PAR_{global}}$. $\mathrm{PAR_{diffuse}}$ increases with increasing k_t, peaking at values of k_t around 0.5 under thin cloud conditions ($0.3 \leq k_t < 0.7$), and then decreases towards clear-sky conditions, at high values of k_t. $\mathrm{PAR_{direct}}$ increases exponentially when the sky starts having clearer conditions ($k_t > 0.3$), and rapidly increases after the $\mathrm{PAR_{diffuse}}$ decreases ($k_t > 0.7$). At high values of k_t, $\mathrm{PAR_{direct}}$ significantly contributes to the $\mathrm{PAR_{global}}$. These trends are consistent across the three studied sites and align with Li et al.'s (2020) findings in a desert environment in the northern hemisphere. However, the magnitude of the $\mathrm{PAR_{global}}$ in this study are halved due to the climate and latitude characteristics.

The analysis demonstrates that the seasonality variation of PAR components and the relationship with cloudiness in high latitudes is similar to mid-latitudes in the northern hemisphere. However, the magnitude of the PAR components decreases as the location moves further north. This decrease is particulary noticeable for the $\mathrm{PAR_{direct}}$ component due to the distinct course of the solar zenith angle throughout the year resulting in reduced solar radiation. The $\mathrm{PAR_{diffuse}}$ component, on the other hand, appears to have minor variability across seasons and locations, indicating that it is less influenced by incoming solar irradiance and more likely to be affected by sky conditions and atmospheric aerosols content.

5. Conclusions

The issue of conflicting land use between agricultural activities and ground-mounted solar photovoltaic power plants has become increasingly prevalent in recent years, and agrivoltaic systems offer a potential solution to this problem. Accurately estimating $PAR_{diffuse}$ is crucial for analysing agrivoltaic systems, as crops situated underneath do not receive PAR_{global} in a uniform manner, as is the case in open-field conditions. Instead, they receive a non-uniform combination of $PAR_{diffuse}$ and PAR_{direct} due to the shading produced by the PV system, with shaded areas receiving a greater proportion of $PAR_{diffuse}$. This shading typically reduces crop yields, making accurate calculation of $PAR_{diffuse}$ essential for more precise crop yield predictions.

To this end, the present study proposes a new separation model called CLY, which calculates $PAR_{diffuse}$ from PAR_{global} using the Yang2 decomposition model for GHI (Yang and Boland, 2019) as a basis. The CLY model leverages atmospheric from satellites, which are widely available worldwide, and utilizes predictors selected through correlation analysis and previous literature findings.

The accuracy of the model has been compared to that of two previously identified best GHI separation models for PAR (Ma Lu et al., 2022), namely Yang2 and Starke, across different locations in Sweden. Results show that the CLY model outperforms both the Yang2 and Starke models in two of the three locations studied. Across all locations, the model achieves R^2 values above 0.91, with an improvement of up to 1% in both R^2 and nRMSE compared to the previously identified most accurate model, Yang2. Although the CLY model has only been validated in three locations at high northern latitude (>58°N), primarily chosen because of the lack of studies in these regions, it could be subject to further studies to investigate its applicability and performance in other climates and at other temporal resolutions.

Acknowledgements

The authors would like to acknowledge the financial support received from the Swedish Energy Agency through the SOLVE project (grant number 52693-1). Additionally, author Pietro Elia Campana would like to acknowledge Formas - the Swedish Research Council for Sustainable Development - for the funding received through the early career project "Avoiding conflicts between the sustainable development goals through agro-photovoltaic systems" (grant number FR-2021/0005). The authors also acknowledge the Swedish Energy Agency for their financial support through the project "Evaluation of the first agrivoltaic system in Sweden" (grant number 51000-1).

The authors would also like to acknowledge ICOS Sweden for providing the data from the Lanna, Degerö, and Norunda stations. ICOS Sweden is funded by the Swedish Research Council as a national research infrastructure. Lastly, the authors would like to thank Dejwakh Kathleen for her assistance in better understanding the satellite-derived data obtained from the NASA Langley Research Center CERES ordering tool at https://ceres.larc.nasa.gov/data/.

CRediT author statement

Silvia Ma Lu: Conceptualization, Methodology, Data Curation, Formal analysis, Validation, Visualization, Writing - Original Draft, Writing - Review & Editing; **Dazhi Yang**: Writing - Review & Editing; **Martha C. Anderson**: Writing - Review & Editing; **Sebastian Zainali**: Writing - Review & Editing; **Bengt Stridh**: Writing - Review & Editing; **Anders Avelin**: Writing - Review & Editing; **Pietro Elia Campana**: Funding acquisition, Conceptualization, Methodology, Writing - Review & Editing.

Appendix

A1. Correlation analysis

Table A - 1 displays the Pearson correlation coefficient (r) between the variables presented in Tables 2 and 3 and the diffuse fraction of PAR. The data used for the correlation analysis and the results in Section 4 were retrieved from the ICOS Sweden Lanna, Degerö and Norunda stations for the years 2016, 2017, and 2018. The Pearson correlation method is the most common way of measuring linear correlations. It assigns a value between -1 and 1, where 0 is no correlation, 1 is total positive correlation, and -1 is total negative correlation (Nettleton, 2014).

The variables that showed high and medium degrees of correlation but were not considered as new predictors for the proposed model could be associated with various reasons. Firstly, these variables were already accounted for or implicitly accounted for in existent significant variables in the YANG2 model (i.e., Swin, PPFD_DIR). Secondly, these variables were accounted for in the calculation of another variable that was considered as a new predictor (e.g., PPFD_IN and PPFD_OUT were used to calculate $\mathrm{PAR}_{\mathrm{albedo}}$. Thirdly, these variables are difficult to obtain if they are not measured on-site (e.g., sunshine duration, H, LE). Lastly, these variables showed minor or scarce influence on PAR (e.g., RH).

Table A - 1. Pearson's correlation coefficient values of the variables investigated to the diffuse fraction of PAR under the studied locations. Highlighted in bold are the variables chosen as predictors for the proposed model.

	Pearson's correlation coefficient (r) to k_{PAR}		
Variable	**Lanna**	**Degerö**	**Norunda**
Swin_p	-0.7617	-0.7233	-0.6872
Lwin	0.2899	0.3843	0.3340
Lwnet	0.8972	0.8767	0.8661
Lwout	-0.4335	-0.3066	-0.2315
NetRad	-0.6602	-0.5460	-0.6111
PPFD_DIFF	-0.0301	0.0650	0.1118
PPFD_DIR	-0.7510	-0.7155	-0.6838
PPFD_IN	-0.7408	-0.7047	-0.6741
PPFD_OUT	-0.3616	-0.2312	-0.6310
P	0.0942	0.1244	0.0869
Pa	-0.1793	-0.2304	-0.1282
RH	0.6266	0.6043	0.4886
Sun	-0.9513	-0.9466	-0.9382
Swin_n	-0.7596	-0.7173	-0.6964
Swnet_n	-0.7475	-0.6486	-0.6905
Swout_n	-0.7015	-0.4157	-0.7419
T_canopy	-0.3718	-0.2865	-0.2294
Ta	-0.3506	-0.2988	-0.2192
H	-0.5964	-	-0.5267
LE	-0.5565	-	-0.3376
Fc	0.3215	-	0.2193
Fn2o	0.1408	-	-
Ustar	-0.1389	-	-0.1520
WS	-0.0177	-	-0.0627
WD	-0.0990	-	-0.0785
NEE	0.3295	-	0.2540
LE_f	-0.5887	-	-0.3575
H_f	-0.6045	-	-0.5378
Alb	0.0437	0.0540	-0.1926
PAR_{albedo}	**0.1360**	**0.1200**	**0.0902**
AM	0.3242	0.2390	0.1960
e_a	0.0524	0.0873	0.1410
e_s	-0.3755	-0.3407	-0.2448
VPD	**-0.5478**	**-0.5329**	**-0.4373**
δ	0.7984	0.7732	0.8153
δ_{PAR}	**0.8111**	**0.7907**	**0.8453**
T_{dew}	0.0300	0.0745	0.1160
AOD	**0.2613**	**0.2353**	**0.2873**

In addition, to aid readers with visualization, the scatterplots of the analysed variables are presented in figures A-1, A-2. The scatterplots provide a graphical representation of the relationships between the variables, allowing readers to observe any trends or patterns that may exist besides linear relationships.

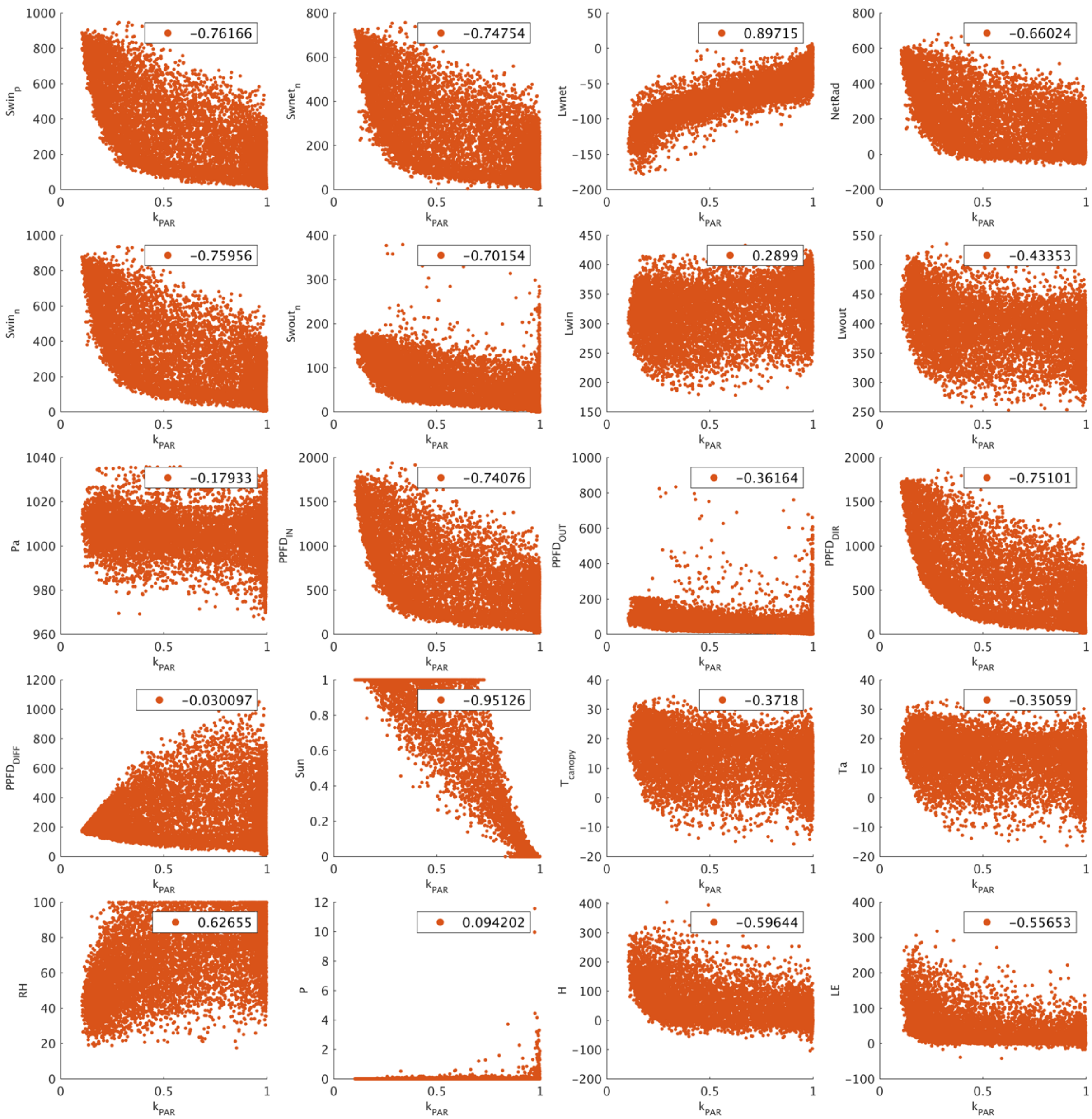

Figure A- 1. Scatterplots of the diffuse fraction of PAR (x-axis) to the variables from Table 2 (y-axis) from Lanna ICOS-Sweden network station for the period 2016-2018. Pearson's correlation coefficient value is displayed for each plot.

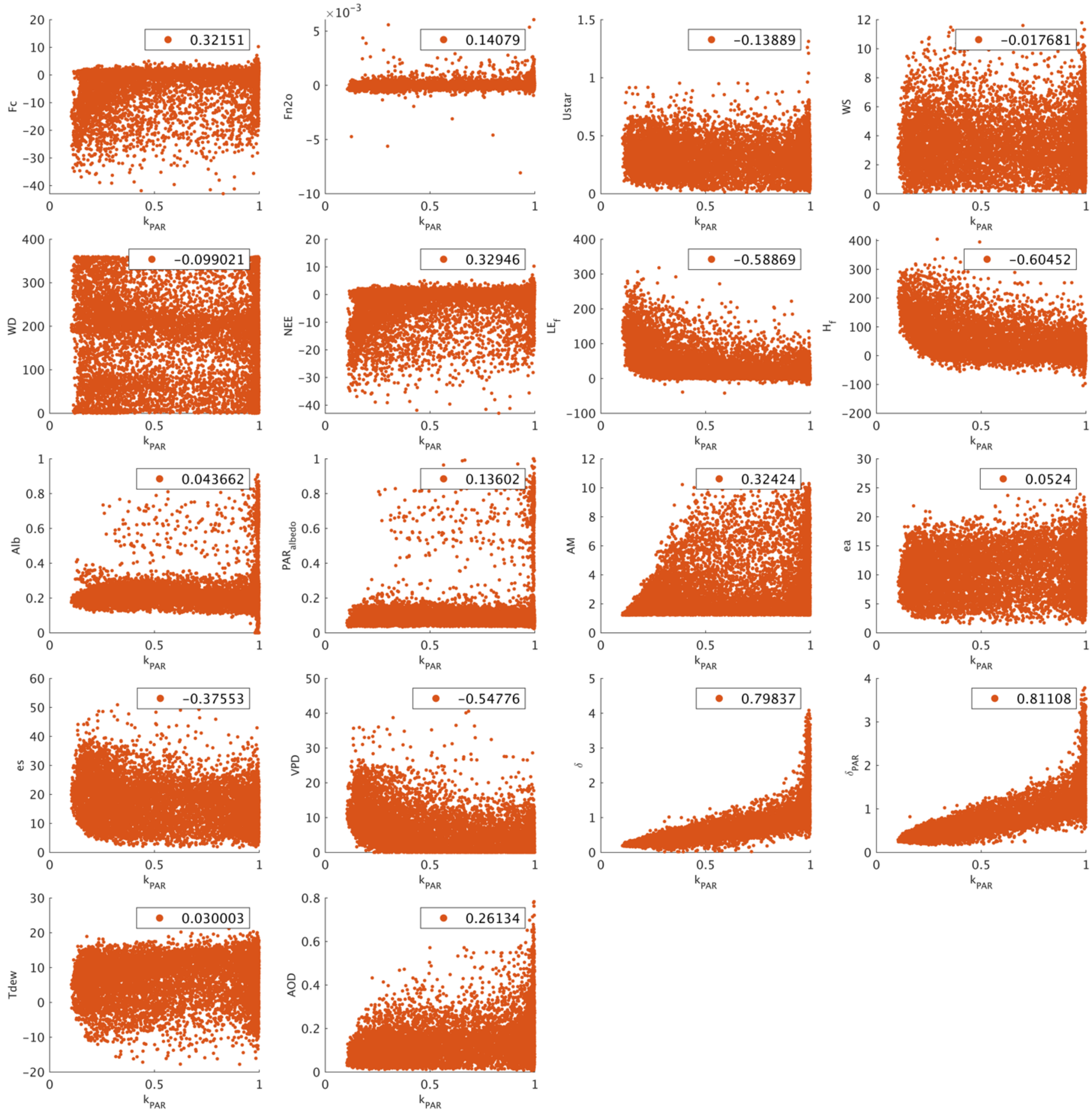

Figure A- 2. (Continuation) Scatterplots of the diffuse fraction of PAR (x-axis) to the variables from Tables 2 and 3 (y-axis) from Lanna ICOS-Sweden network station for the period 2016-2018. Pearson's correlation coefficient value is displayed for each plot.

References

Adeh, E.H., Good, S.P., Calaf, M., Higgins, C.W., 2019. Solar PV Power Potential is Greatest Over Croplands. Sci. Rep. 9, 11442. https://doi.org/10.1038/s41598-019-47803-3

Akitsu, T., Kume, A., Hirose, Y., Ijima, O., Nasahara, K.N., 2015. On the stability of radiometric ratios of photosynthetically active radiation to global solar radiation in Tsukuba, Japan. Agric. For. Meteorol. 209–210, 59–68. https://doi.org/10.1016/j.agrformet.2015.04.026

Aladros, I., Foyo-Moreno, I., Alados-Arboledas, L., 1996. Photosynthetically active radiation: measurements and modelling. Agric. For. Meteorol. 78, 121–131. https://doi.org/10.1016/0168-1923(95)02245-7

Barenbrug, A.W.T., 1974. Psychrometry and psychrometric charts, 3d ed. ed. Chamber of Mines of South Africa, Johannesburg.

Barron-Gafford, G.A., Pavao-Zuckerman, M.A., Minor, R.L., Sutter, L.F., Barnett-Moreno, I., Blackett, D.T., Thompson, M., Dimond, K., Gerlak, A.K., Nabhan, G.P., Macknick, J.E., 2019. Agrivoltaics provide mutual benefits across the food–energy–water nexus in drylands. Nat. Sustain. 2, 848–855. https://doi.org/10.1038/s41893-019-0364-5

Bird, R.E., Riordan, C., 1986. Simple Solar Spectral Model for Direct and Diffuse Irradiance on Horizontal and Tilted Planes at the Earth's Surface for Cloudless Atmospheres. J. Clim. Appl. Meteorol. 25, 87–97. https://doi.org/10.1175/1520-0450(1986)025<0087:SSSMFD>2.0.CO;2

Campana, P.E., Stridh, B., Amaducci, S., Colauzzi, M., 2021. Optimisation of vertically mounted agrivoltaic systems. J. Clean. Prod. 325, 129091. https://doi.org/10.1016/j.jclepro.2021.129091

Chen, J., Shen, M., Kato, T., 2009. Diurnal and seasonal variations in light-use efficiency in an alpine meadow ecosystem: causes and implications for remote sensing. J. Plant Ecol. 2, 173–185. https://doi.org/10.1093/jpe/rtp020

de Blas, M., García-Rodríguez, A., García, I., Torres, J.L., 2022. Validation and calibration of models to estimate photosynthetically active radiation considering different time scales and sky conditions. Adv. Space Res. 70, 1737–1760. https://doi.org/10.1016/j.asr.2022.07.005

Doelling, D., 2017. CERES Level 3 SYN1deg-1Hour Terra-Aqua-MODIS HDF4 file - Edition 4A. https://doi.org/10.5067/TERRA+AQUA/CERES/SYN1DEG-1HOUR_L3.004A

Duffie, J.A., Beckman, W.A., 2013. Solar engineering of thermal processes / John A. Duffie, William A. Beckman, 4th ed. ed. John Wiley, Hoboken.

ECMWF, 2022. CAMS-AOD [WWW Document]. SoDa. URL https://www.soda-pro.com/web-services/atmosphere/cams-aod (accessed 10.20.22).

Emde, C., Buras-Schnell, R., Kylling, A., Mayer, B., Gasteiger, J., Hamann, U., Kylling, J., Richter, B., Pause, C., Dowling, T., Bugliaro, L., 2016. The libRadtran software package for radiative transfer calculations (version 2.0.1). Geosci. Model Dev. 9, 1647–1672. https://doi.org/10.5194/gmd-9-1647-2016

Ferrera-Cobos, F., Vindel, J.M., Valenzuela, R.X., González, J.A., 2020. Analysis of Spatial and Temporal Variability of the PAR/GHI Ratio and PAR Modeling Based on Two Satellite Estimates. Remote Sens. 12, 1262. https://doi.org/10.3390/rs12081262

GADM, 2022. GADM [WWW Document]. GADM. URL https://www.gadm.org (accessed 5.2.20).

García-Rodríguez, A., García-Rodríguez, S., Díez-Mediavilla, M., Alonso-Tristán, C., 2020. Photosynthetic Active Radiation, Solar Irradiance and the CIE Standard Sky Classification. Appl. Sci. 10, 8007. https://doi.org/10.3390/app10228007

Gneiting, T., 2011. Making and Evaluating Point Forecasts. J. Am. Stat. Assoc. 106, 746–762. https://doi.org/10.1198/jasa.2011.r10138

González, J.A., Calbó, J., 2002. Modelled and measured ratio of PAR to global radiation under cloudless skies. Agric. For. Meteorol. 110, 319–325. https://doi.org/10.1016/S0168-1923(01)00291-X

Gu, L., Baldocchi, D., Verma, S.B., Black, T.A., Vesala, T., Falge, E.M., Dowty, P.R., 2002. Advantages of diffuse radiation for terrestrial ecosystem productivity: ADVANTAGES OF DIFFUSE RADIATION. J. Geophys. Res. Atmospheres 107, ACL 2-1-ACL 2-23. https://doi.org/10.1029/2001JD001242

Gu, L., Fuentes, J.D., Shugart, H.H., Staebler, R.M., Black, T.A., 1999. Responses of net ecosystem exchanges of carbon dioxide to changes in cloudiness: Results from two North American deciduous forests. J. Geophys. Res. Atmospheres 104, 31421–31434. https://doi.org/10.1029/1999JD901068

Gueymard, C., 1995. Simple Model for the Atmospheric Radiative Transfer of Sunshine (SMARTS2) Algorithms and performance assessment 84.

Gueymard, C.A., 2018. A reevaluation of the solar constant based on a 42-year total solar irradiance time series and a reconciliation of spaceborne observations. Sol. Energy 168, 2–9. https://doi.org/10.1016/j.solener.2018.04.001

Hao, D., Asrar, G.R., Zeng, Y., Zhu, Q., Wen, J., Xiao, Q., Chen, M., 2019. Estimating hourly land surface downward shortwave and photosynthetically active radiation from DSCOVR/EPIC observations. Remote Sens. Environ. 232, 111320. https://doi.org/10.1016/j.rse.2019.111320

Hu, B., Wang, Y., Liu, G., 2007. Spatiotemporal characteristics of photosynthetically active radiation in China. J. Geophys. Res. 112, D14106. https://doi.org/10.1029/2006JD007965

ICOS Sweden [WWW Document], 2022. URL https://www.icos-sweden.se/ (accessed 10.6.22).

Iqbal, M., 1983. An Introduction to Solar Radiation. Elsevier. https://doi.org/10.1016/B978-0-12-373750-2.X5001-0

Jacovides, C.P., Boland, J., Asimakopoulos, D.N., Kaltsounides, N.A., 2010. Comparing diffuse radiation models with one predictor for partitioning incident PAR radiation into its diffuse component in the eastern Mediterranean basin. Renew. Energy 35, 1820–1827. https://doi.org/10.1016/j.renene.2009.11.015

Jacovides, C.P., Tymvios, F.S., Asimakopoulos, D.N., Theofilou, K.M., Pashiardes, S., 2003. Global photosynthetically active radiation and its relationship with global solar radiation in the Eastern Mediterranean basin. Theor. Appl. Climatol. 74, 227–233. https://doi.org/10.1007/s00704-002-0685-5

Janjai, S., Wattan, R., 2011. Development of a model for the estimation of photosynthetically active radiation from geostationary satellite data in a tropical environment. Remote Sens. Environ. 115, 1680–1693. https://doi.org/10.1016/j.rse.2011.02.026

Kanniah, K.D., Beringer, J., North, P., Hutley, L., 2012. Control of atmospheric particles on diffuse radiation and terrestrial plant productivity: A review. Prog. Phys. Geogr. Earth Environ. 36, 209–237. https://doi.org/10.1177/0309133311434244

Kasten, F., Young, A.T., 1989. Revised optical air mass tables and approximation formula. Appl. Opt. 28, 4735. https://doi.org/10.1364/AO.28.004735

Kathilankal, J.C., O’Halloran, T.L., Schmidt, A., Hanson, C.V., Law, B.E., 2014. Development of a semi-parametric PAR (Photosynthetically Active Radiation) partitioning model for the United States, version 1.0. Geosci. Model Dev. 7, 2477–2484. https://doi.org/10.5194/gmd-7-2477-2014

Keane, B.J., Ineson, P., Vallack, H.W., Blei, E., Bentley, M., Howarth, S., McNamara, N.P., Rowe, R.L., Williams, M., Toet, S., 2018. Greenhouse gas emissions from the energy crop oilseed rape (*Brassica napus*); the role of photosynthetically active radiation in diurnal N_2O flux variation. GCB Bioenergy 10, 306–319. https://doi.org/10.1111/gcbb.12491

Koblick, D., 2021. Vectorized Solar Azimuth and Elevation Estimation [WWW Document]. MATLAB Cent. File Exch. URL https://se.mathworks.com/matlabcentral/fileexchange/23051-vectorized-solar-azimuth-and-elevation-estimation (accessed 12.9.21).

Langhans, R.W., Tibbitts, T.W., Use, N.C.R.C.N.-101 on C.E.T. and, 1997. Plant Growth Chamber Handbook. Iowa Agricultural and Home Economics Experiment Station.

Li, C., Jia, X., Ma, J., Liu, P., Yang, R., Bai, Y., Hayat, M., Liu, J., Zha, T., 2020. Linking diffuse radiation and ecosystem productivity of a desert steppe ecosystem. PeerJ 8, e9043. https://doi.org/10.7717/peerj.9043

Li, R., Zhao, L., Ding, Y., Wang, S., Ji, G., Xiao, Y., Liu, G., Sun, L., 2010. Monthly ratios of PAR to global solar radiation measured at northern Tibetan Plateau, China. Sol. Energy 84, 964–973. https://doi.org/10.1016/j.solener.2010.03.005

Lozano, I.L., Sánchez-Hernández, G., Guerrero-Rascado, J.L., Alados, I., Foyo-Moreno, I., 2022. Analysis of cloud effects on long-term global and diffuse photosynthetically active radiation at a Mediterranean site. Atmospheric Res. 268, 106010. https://doi.org/10.1016/j.atmosres.2021.106010

Lu, H., Qin, Z., Lin, S., Chen, X., Chen, B., He, B., Wei, J., Yuan, W., 2022. Large influence of atmospheric vapor pressure deficit on ecosystem production efficiency. Nat. Commun. 13, 1653. https://doi.org/10.1038/s41467-022-29009-w

Ma Lu, S., Zainali, S., Campana, P., Stridh, B., Avelin, A., Amaducci, S., Colauzzi, M., 2022. Photosynthetically Active Radiation Decomposition Models for Agrivoltaic Systems Applications (preprint). Bioresource and Agricultural Engineering. https://doi.org/10.31223/X5JK9N

Mariscal, MariaJ., Martens, ScottN., Ustin, SusanL., Chen, J., Weiss, StuartB., Roberts, DarA., 2004. Light-transmission Profiles in an Old-growth Forest Canopy:Simulations of Photosynthetically Active Radiation by Using Spatially Explicit Radiative Transfer Models. Ecosystems 7. https://doi.org/10.1007/s10021-004-0137-4

McCree, K.J., 1972. Test of current definitions of photosynthetically active radiation against leaf photosynthesis data. Agric. Meteorol. 10, 443–453. https://doi.org/10.1016/0002-1571(72)90045-3

McCree, K.J., 1971. The action spectrum, absorptance and quantum yield of photosynthesis in crop plants. Agric. Meteorol. 9, 191–216. https://doi.org/10.1016/0002-1571(71)90022-7

Mercado, L.M., Bellouin, N., Sitch, S., Boucher, O., Huntingford, C., Wild, M., Cox, P.M., 2009. Impact of changes in diffuse radiation on the global land carbon sink. Nature 458, 1014–1017. https://doi.org/10.1038/nature07949

Mizoguchi, Y., Ohtani, Y., Aoshima, T., Hirakata, A., Yuta, S., Takanashi, S., Iwata, H., Nakai, Y., 2010. Comparison of the characteristics of five quantum sensors. Bull. FFPRI 9, 113–120.

Nettleton, D., 2014. Selection of Variables and Factor Derivation, in: Commercial Data Mining. Elsevier, pp. 79–104. https://doi.org/10.1016/B978-0-12-416602-8.00006-6

Niu, Z., Wang, L., Niu, Y., Hu, B., Zhang, M., Qin, W., 2019. Spatiotemporal variations of photosynthetically active radiation and the influencing factors in China from 1961 to 2016. Theor. Appl. Climatol. 137, 2049–2067. https://doi.org/10.1007/s00704-018-2727-7

Noriega Gardea, M.M.A., Corral Martínez, L.F., Anguiano Morales, M., Trujillo Schiaffino, G., Salas Peimbert, D.P., 2020. MODELLING PHOTOSYNTHETICALLY ACTIVE RADIATION: A REVIEW. Atmósfera. https://doi.org/10.20937/ATM.52737

Nwokolo, S., 2018. A Global Review of Empirical Models for Estimating Photosynthetically Active Radiation. Trends Renew. Energy 4. https://doi.org/10.17737/tre.2018.4.2.0079

Oliphant, A.J., Stoy, P.C., 2018. An Evaluation of Semiempirical Models for Partitioning Photosynthetically Active Radiation Into Diffuse and Direct Beam Components. J. Geophys. Res. Biogeosciences 123, 889–901. https://doi.org/10.1002/2017JG004370

Olseth, J., 1997. Spatial distribution of photosynthetically active radiation over complex topography. Agric. For. Meteorol. 86, 205–214. https://doi.org/10.1016/S0168-1923(97)00010-5

Proutsos, N.D., Liakatas, A., Alexandris, S.G., Tsiros, I.X., Tigkas, D., Halivopoulos, G., 2022. Atmospheric Factors Affecting Global Solar and Photosynthetically Active Radiation Relationship in a Mediterranean Forest Site. Atmosphere 13, 1207. https://doi.org/10.3390/atmos13081207

Räisänen, J., 2019. Energetics of interannual temperature variability. Clim. Dyn. 52, 3139–3156. https://doi.org/10.1007/s00382-018-4306-0

Ren, X., He, H., Zhang, L., Yu, G., 2018. Global radiation, photosynthetically active radiation, and the diffuse component dataset of China, 1981–2010. Earth Syst. Sci. Data 10, 1217–1226. https://doi.org/10.5194/essd-10-1217-2018

Ridley, B., Boland, J., Lauret, P., 2010. Modelling of diffuse solar fraction with multiple predictors. Renew. Energy 35, 478–483. https://doi.org/10.1016/j.renene.2009.07.018

Sinclair, V.A., Mikkola, J., Rantanen, M., Räisänen, J., 2019. The summer 2018 heatwave in Finland. Weather 74, 403–409. https://doi.org/10.1002/wea.3525

Spencer, J. W, 1971. Fourier Series Representation of the Position of the Sun. Search 2, 172.

Spitters, C.J.T., Toussaint, H.A.J.M., Goudriaan, J., 1986. Separating the diffuse and direct component of global radiation and its implications for modeling canopy photosynthesis Part I. Components of incoming radiation. Agric. For. Meteorol. 38, 217–229. https://doi.org/10.1016/0168-1923(86)90060-2

Starke, A.R., Lemos, L.F.L., Boland, J., Cardemil, J.M., Colle, S., 2018. Resolution of the cloud enhancement problem for one-minute diffuse radiation prediction. Renew. Energy 125, 472–484. https://doi.org/10.1016/j.renene.2018.02.107

Su, W., Charlock, T.P., Rose, F.G., Rutan, D., 2007. Photosynthetically active radiation from Clouds and the Earth's Radiant Energy System (CERES) products. J. Geophys. Res. 112, G02022. https://doi.org/10.1029/2006JG000290

Tan, C., Wang, D., Zhou, J., Du, Y., Luo, M., Zhang, Y., Guo, W., 2018. Remotely Assessing Fraction of Photosynthetically Active Radiation (FPAR) for Wheat Canopies Based on Hyperspectral Vegetation Indexes. Front. Plant Sci. 9, 776. https://doi.org/10.3389/fpls.2018.00776

Technical Committee on Standardization of Reference Evapotranspiration, 2005. The ASCE Standardized Reference Evapotranspiration Equation. American Society of Civil Engineers, Reston, VA. https://doi.org/10.1061/9780784408056

Thomas, C., Dorling, S., Wandji Nyamsi, W., Wald, L., Rubino, S., Saboret, L., Trolliet, M., Wey, E., 2019. Assessment of five different methods for the estimation of surface photosynthetically active radiation from satellite imagery at three sites – application to the monitoring of indoor soft fruit crops in southern UK. Adv. Sci. Res. 16, 229–240. https://doi.org/10.5194/asr-16-229-2019

Trisolino, P., di Sarra, A., Anello, F., Bommarito, C., Di Iorio, T., Meloni, D., Monteleone, F., Pace, G., Piacentino, S., Sferlazzo, D., 2018. A long-term time series of global and diffuse photosynthetically active radiation in the Mediterranean: interannual variability and cloud effects. Atmospheric Chem. Phys. 18, 7985–8000. https://doi.org/10.5194/acp-18-7985-2018

Trisolino, P., Sarra, A. di, Meloni, D., Pace, G., 2016. Determination of global and diffuse photosynthetically active radiation from a multifilter shadowband radiometer. Appl. Opt. 55, 8280. https://doi.org/10.1364/AO.55.008280

US Department of Commerce, N., 2021. ESRL Global Monitoring Laboratory - Global Radiation and Aerosols [WWW Document]. URL https://gml.noaa.gov/grad/solcalc/calcdetails.html (accessed 12.14.21).

Wandji Nyamsi, W., Blanc, P., Augustine, J.A., Arola, A., Wald, L., 2019. A New Clear-Sky Method for Assessing Photosynthetically Active Radiation at the Surface Level. Atmosphere 10, 219. https://doi.org/10.3390/atmos10040219

Wang, L., Kisi, O., Zounemat-Kermani, M., Hu, B., Gong, W., 2016. Modeling and comparison of hourly photosynthetically active radiation in different ecosystems. Renew. Sustain. Energy Rev. 56, 436–453. https://doi.org/10.1016/j.rser.2015.11.068

Wang, Q., Tenhunen, J., Schmidt, M., Kolcun, O., Droesler, M., Reichstein, M., 2006. Estimation of total, direct and diffuse PAR under clear skies in complex alpine terrain of the National Park Berchtesgaden, Germany. Ecol. Model. 196, 149–162. https://doi.org/10.1016/j.ecolmodel.2006.02.005

Weiss, A., Norman, J.M., 1985. Partitioning solar radiation into direct and diffuse, visible and near-infrared components. Agric. For. Meteorol. 34, 205–213. https://doi.org/10.1016/0168-1923(85)90020-6

Wielicki, B.A., Barkstrom, B.R., Harrison, E.F., Lee, R.B., Louis Smith, G., Cooper, J.E., 1996. Clouds and the Earth's Radiant Energy System (CERES): An Earth Observing System Experiment. Bull. Am. Meteorol. Soc. 77, 853–868. https://doi.org/10.1175/1520-0477(1996)077<0853:CATERE>2.0.CO;2

Wilcke, R.A.I., Kjellström, E., Lin, C., Matei, D., Moberg, A., Tyrlis, E., 2020. The extremely warm summer of 2018 in Sweden – set in a historical context. Earth Syst. Dyn. 11, 1107–1121. https://doi.org/10.5194/esd-11-1107-2020

Yang, D., Alessandrini, S., Antonanzas, J., Antonanzas-Torres, F., Badescu, V., Beyer, H.G., Blaga, R., Boland, J., Bright, J.M., Coimbra, C.F.M., David, M., Frimane, Â., Gueymard, C.A., Hong, T., Kay, M.J., Killinger, S., Kleissl, J., Lauret, P., Lorenz, E., van der Meer, D., Paulescu, M., Perez, R., Perpiñán-Lamigueiro, O., Peters, I.M., Reikard, G., Renné, D., Saint-Drenan, Y.-M., Shuai, Y., Urraca, R., Verbois, H., Vignola, F., Voyant, C., Zhang, J., 2020. Verification of deterministic solar forecasts. Sol. Energy 210, 20–37. https://doi.org/10.1016/j.solener.2020.04.019

Yang, D., Boland, J., 2019. Satellite-augmented diffuse solar radiation separation models. J. Renew. Sustain. Energy 11, 023705. https://doi.org/10.1063/1.5087463

Yang, D., Kleissl, J., 2022. Summarizing ensemble NWP forecasts for grid operators: Consistency, elicitability, and economic value. Int. J. Forecast. S016920702200111X. https://doi.org/10.1016/j.ijforecast.2022.08.002

Yu, X., Guo, X., 2016. Hourly photosynthetically active radiation estimation in Midwestern United States from artificial neural networks and conventional regressions models. Int. J. Biometeorol. 60, 1247–1259. https://doi.org/10.1007/s00484-015-1120-9

Yu, X., Wu, Z., Jiang, W., Guo, X., 2015. Predicting daily photosynthetically active radiation from global solar radiation in the Contiguous United States. Energy Convers. Manag. 89, 71–82. https://doi.org/10.1016/j.enconman.2014.09.038